Dalton Transactions

PAPER

View Article Online
View Journal | View Issue

Cite this: *Dalton Trans.*, 2016, **45**, 17714

Reduction of hypervalent iodine by coordination to iron(III) and the crystal structures of PhIO and $PhIO_2$†

Christina Wegeberg,[a] Christian Grundahl Frankær[b] and Christine J. McKenzie*[a]

The iodine L_3-edge X-ray Absorption Near Edge Structure (XANES) of organic and inorganic iodine compounds with formal iodine oxidation states ranging from –1 to +7 shows edge energies spanning from 4560.8 eV to 4572.5 eV. These were used to calibrate the oxidation state of iodine in a unique iron complex of iodosylbenzene (PhIO), $[Fe(tpena)OIPh]^{2+}$ ($tpena^-$ = *N*,*N*,*N*′-tris(2-pyridylmethyl)ethylenediamine-*N*′-acetate), which was found to be +1.6. Thus the iodine oxidation state is reduced by 1.4 compared with that in precursor uncoordinated PhIO. On the basis of a combination of X-ray diffraction and Extended X-ray Absorption Fine Structure (EXAFS) spectroscopy, we have determined the unknown crystal structure of PhIO, along with a new phase of iodylbenzene (β-$PhIO_2$) using the Rietveld method. Analogous 1-D chains of halogen bonded [···O–I···O–I] motifs are the dominant supramolecular interactions between PhIO and $PhIO_2$ monomers in each structure respectively and the polymeric structures rationalise the general insolubility of these oxygen atom transfer reagents. A double stack of phenyl units in PhIO is found between the layers of the halogen bonded O/I chains. In the case of PhIO, C–H···π interactions between adjacent phenyl groups result in the alternate phenyl groups lying in parallel planes. Supplementing the strong polymerizing halogen bonds, this supramolecular interaction must exacerbate the insolubility of PhIO. The pillared structure of the new rhombohedral β-$PhIO_2$ differs significantly from the known monoclinic lamellar phase, α-$PhIO_2$, described 36 years ago in which the chains form lamellar stacks [N. W. Alcock and J. F. Sawyer, *J. Chem. Soc., Dalton Trans.*, 1980, 115–120].

Received 25th July 2016,
Accepted 5th October 2016

DOI: 10.1039/c6dt02937j

www.rsc.org/dalton

Introduction

Despite already being six coordinated by the hexadentate ligand, the iron(III) complex of *N*,*N*,*N*′-tris(2-pyridylmethyl)ethylenediamine-*N*′-acetate $[Fe(tpena)]^{2+}$ solubilizes the otherwise "insoluble" iodosylbenzene (PhIO). It is proposed that the high-spin diastereomeric form of this complex extracts a monomer from the "polymeric" solid thereby forming the seven coordinated complex, $[Fe(tpena)OIPh]^{2+}$.[1] This complex is the only structurally characterized metal complex containing a PhIO ligand[2] and is a landmark compound with respect to the activation of this oxygen transfer agent in catalysis. The structure of $[Fe(tpena)OIPh](ClO_4)_2$ shows that the dications are dimerized through multiple and strong halogen-bonding interactions to form $[Fe(tpena)OIPh]_2^{4+}$, Fig. 1(a). Non-bonding intradimer I···O distances are up to 1 Å shorter than the sum of the van der Waals radii of O and I, and the shortest of them is by a relatively large margin the shortest non-covalent O···I interaction in the Cambridge Structural Database (CSD).[3]

The strong halogen bonding has presumably enabled the solid state trapping of this novel species. In the context of elucidation of the mechanism of the catalysis of sulfoxidation and epoxidation by $[Fe(tpena)]^{2+}$, the question is now whether the direct O-transfer agent in the catalytic cycle is the $[Fe(tpena)OIPh]^{2+}$ adduct (in its dimeric or monomeric form), or a hypervalent iron(IV) or iron(V) derivative (Fig. 1b). Consideration of how metal ion coordination affects the electronic structure of the PhIO ligand, and the iron atom, respectively, will furnish information towards answering this question. To determine how much inner sphere charge transfer has occurred during PhIO coordination, it is therefore obvious to compare the I–O bond length in free *vs*. coordinated PhIO: a tendency towards increasing oxidation state of the iron with

[a]*Department of Physics, Chemistry and Pharmacy, University of Southern Denmark, Campusvej 55, 5230 Odense M, Denmark. E-mail: mckenzie@sdu.dk; Fax: (+45) 6615 8760; Tel: +45 6550 2518*
[b]*Department of Chemistry, Technical University of Denmark, DK-2800, Kongens Lyngby, Denmark*

†Electronic supplementary information (ESI) available: Details of XANES, bond angles for the intramolecular O–I–O and C–I–O moiety of 23 iodyl compounds extracted from the CCDC, diffractogram of an aged sample of PhIO and NMR spectra of disproportionated and depolymerized PhIO obtained by "dissolution" in dmso-d_6. CCDC 1506866 and 1506867. For ESI and crystallographic data in CIF or other electronic format see DOI: 10.1039/c6dt02937j

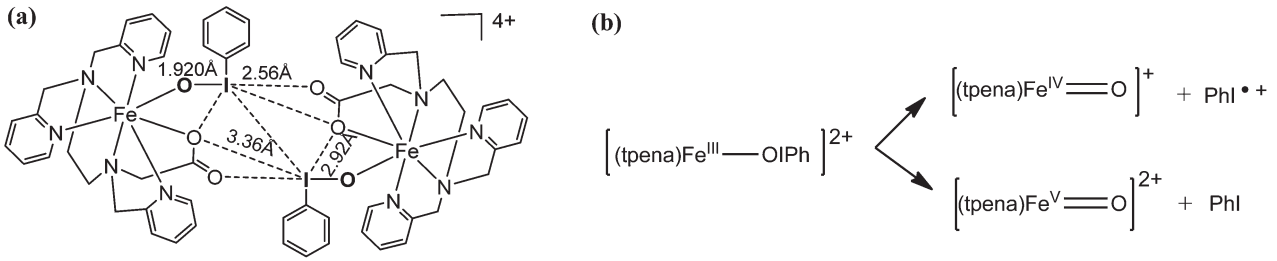

Fig. 1 (a)Intramolecular I–O distances and intermolecular halogen-bonded I···O distances in the dimers of cations in $[Fe(tpena)OIPh](ClO_4)_2$ determined by single crystal X-ray diffraction. (b) The monomeric Fe–OIPh complex as a "protected" form of a more reactive ferryl or perferryl species generated by homolytic and heterolytic FeO–IPh cleavage respectively.

concomitant decrease in the oxidation state of the iodine, should be reflected by an increased FeO–IPh distance in the complex *vs.* its counterpart in "free" PhIO. A relatively short Fe–OIPh distance would also be pertinent. Unfortunately a direct comparison of the I–O bond lengths in free *vs.* coordinated PhIO is not possible, since, despite the fact that this compound has been known for more than a century,[4] its crystal structure is as yet unknown. Several representations of PhIO can be found in the literature: from monomeric, with a double I=O bond and trigonal, linear or L-shaped geometry around the I atom (Fig. 2a), to polymeric due to strong secondary O–I bonds (aka halogen bonding). A structural model with two O–I distances of 2.04 Å and 2.377 Å and an I–O–I angle of 114° was determined on the basis of iodine K-edge EXAFS spectroscopy (Fig. 2b).[5] A C–I–O angle was determined to be close to 90° by Mössbauer spectroscopy.[6] The shortest of the I–O distances is 0.12 Å longer than that in $[Fe(tpena)OIPh]^{2+}$, seemingly incongruent with the notion that this bond should be moving in the direction of homo- or heterolytic cleavage in the iron complex. Solid state interactions will naturally attenuate these distances and these are at best, poorly described in the case of PhIO. For $[Fe(tpena)OIPh]^{2+}$, the interaction of the iodine atom with four oxygen atoms is well defined by structural analysis by single crystal X-ray diffraction (SCXRD).[2]

In an attempt to analyze the charge distribution in $[Fe(tpena)OIPh](ClO_4)_2$, we describe here the determination of the oxidation states of the iodine atoms in $[Fe(tpena)OIPh](ClO_4)_2$ and precursor PhIO using iodine L_3-edge X-ray Absorption Near Edge Structure (XANES) spectroscopy. We have used the most extensive analysis of iodine reference compounds, spanning the −1 to +7 oxidation state range, performed to date. In addition the crystal structures of PhIO and a new phase of $PhIO_2$, hereafter β-$PhIO_2$, determined by combining results from powder X-ray diffraction, XANES and EXAFS are described.

Results and discussion

Iodine L_3-edge XANES of compounds with iodine in formal oxidation states −1 to +7

The iodine L_3-edge XANES spectra of $[Fe(tpena)OIPh](ClO_4)_2$ and the reference compounds listed in Table 1 were recorded in fluorescence mode on neat samples. Edge energies are spread evenly in the range from 4560.8 eV (oxidation state −1) to 4572.0 eV (oxidation state +7) (Fig. 3a). The expected oxidation states for the reference compounds were confirmed and well defined by the steepest inflection point, *i.e.* highest peak in the first derivative spectrum (ESI Fig. S1†). Edges for compounds with the same oxidation state are found to be close in energy despite significantly different geometries around the iodine atoms. For example the compounds with the iodine atom in the oxidation state +5 show similar edge energies (E = 4569.2(7) eV) and are not markedly affected by the iodine atom having three, four or five bonded neighbors or by the nature of these neighboring atoms (ESI Fig. S2†). Linear correlations between the energies of the iodine L_3-edge and L_3-pre-edge and the oxidation states are observed (Fig. 3b). The high oxidation state purely inorganic compounds (KIO_3, $NaIO_4$, H_5IO_6) show relatively more structure in their edges.

The oxidation state of iodine in iron(III)-coordinated PhIO

The iodine L_3-edge for $[Fe(tpena)OIPh](ClO_4)_2$ was found at 4564.4 eV. This is a clear shift to lower energy compared to the edge observed for PhIO (4565.6 eV). By employing the linear

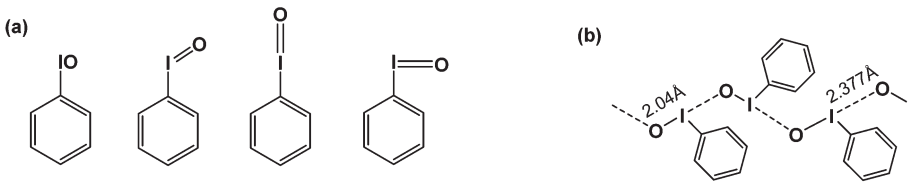

Fig. 2 (a) Various representations of the molecular PhIO found in the literature. (b) Intra- and intermolecular I–O distances in solid state PhIO proposed on the basis of EXAFS.[5]

Table 1 Chemical structures of reference iodine compounds grouped according to their formal iodine oxidation state

Oxidation state	Compound
−1	KI
−1/3	$(TBA)I_3$
0	I_2
+1	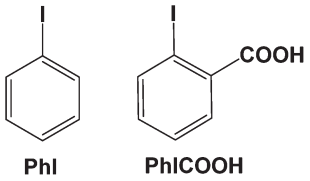 PhI PhICOOH
+3	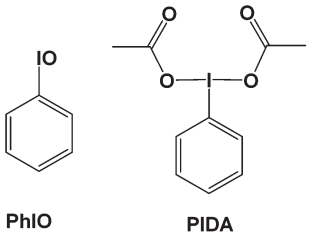 PhIO PIDA
+5	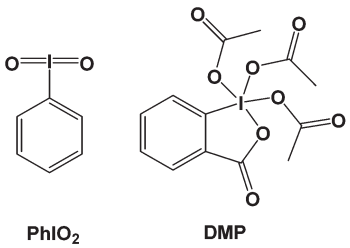 $PhIO_2$ DMP
	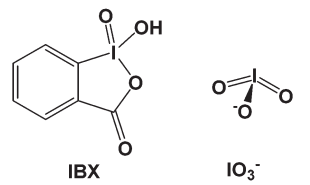 IBX IO_3^-
+7	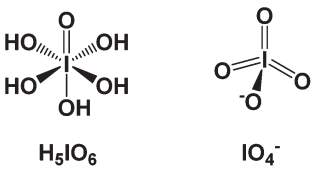 H_5IO_6 IO_4^-

Abbreviations for organic compound are: TBA: *N*-tetrabutylammonium, PhI: phenyl iodide, PhICOOH: 2-iodobenzoic acid, PhIO: iodosylbenzene, PIDA: phenyliodine diacetate, $PhIO_2$: iodylbenzene, DMP: Dess–Martin periodinane and IBX: 2-iodoxybenzoic acid.

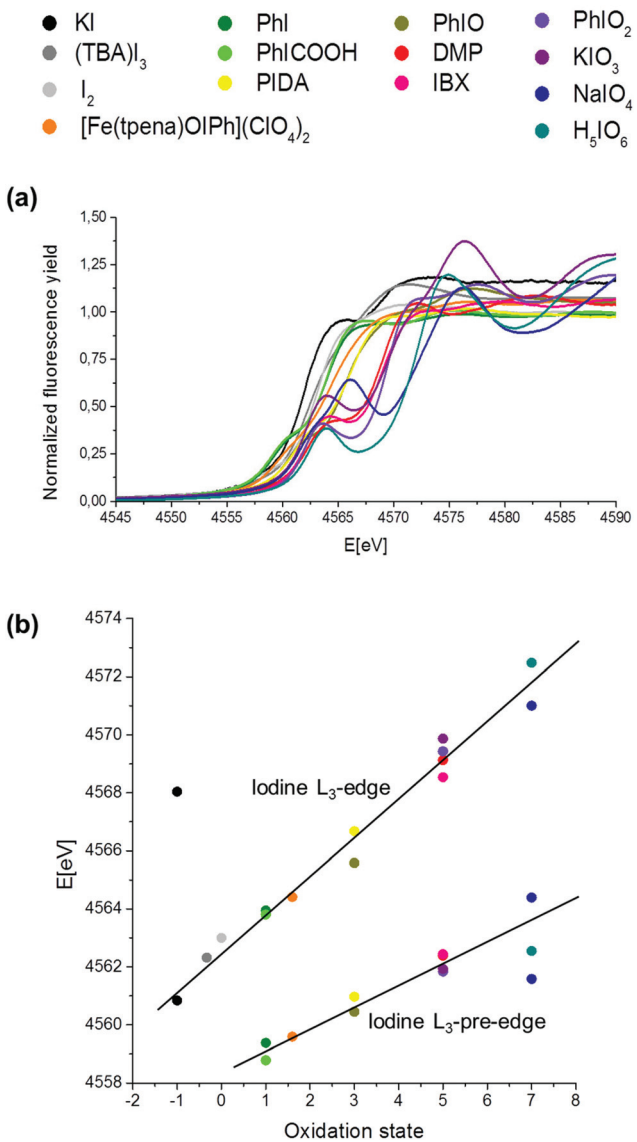

Fig. 3 (a) L_3-edge XANES spectra for the series of compounds containing iodine in the −1 to +7 oxidation states. (b) Trend in iodine L_3-edge and pre-edge XANES. The energies are listed in Table S1.†

correlation shown in Fig. 3b, an iodine oxidation state of +1.6 is indicated. The symmetry of the dimeric structure found by SCXRD (Fig. 2a) speaks against this alternatively representing the average oxidation state in a mixed valent material (*e.g.* I^0/I^{III} or I^I/I^{II}). The reduction of the iodine in the iron complex compared with the starting PhIO (+3) suggests that a considerable charge transfer has occurred on coordination. This apparently does not involve the iron atom since iron K-edge XANES measurements performed on the same sample as used for the iodine L_3-edge measurements[7] are consistent with Fe(III) (7121.5 eV, ESI Fig. S3†) and accords with earlier ^{57}Fe Mössbauer spectroscopy showing that the seven-coordinated iron atom in $[Fe(tpena)OIPh](ClO_4)_2$ is high spin iron(III) (broad singlet, δ = 0.61 mm s^{-1}).[1] Thus there is no tendency toward a higher iron oxidation state than +3 in $[Fe(tpena)OIPh](ClO_4)_2$ and the inner sphere charge transfer involves predominantly the I and O atoms of the coordinated iodosyl-group and possibly also the halogen-bonded carboxylato O atoms.

The crystal structures of PhIO, α-$PhIO_2$ and β-$PhIO_2$

Despite the literature descriptions of PhIO being amorphous,[5] we were able to obtain Powder X-ray Diffraction (PXRD) patterns for freshly synthesized pale yellow PhIO, Fig. 4a, reveal-

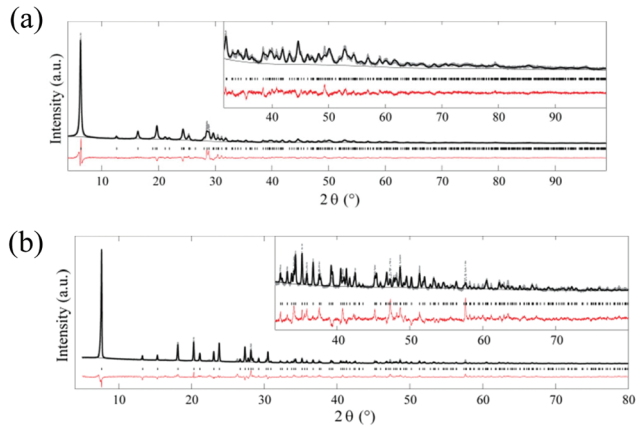

Fig. 4 XRPD patterns (black) and Rietveld plots (red) of (a) PhIO and (b) β-$PhIO_2$. Insets: Magnification of the pattern for $2\theta > 30°$.

ing crystalline materials. Apart from a bigger unit cell volume, the resemblance to the diffraction pattern that can be calculated from the single crystal data for monoclinic $PhIO_2$ [8] (hereafter referred to as α-$PhIO_2$, ESI Fig. S4†), is striking. Disconcertingly, the PXRD patterns of our sample of white $PhIO_2$, Fig. 4b, are significantly different from that calculated for α-$PhIO_2$. By simulated annealing using a fragment of the α-$PhIO_2$ structure and combining this information with distances obtained from the iodine L_3-edge EXAFS data, a new rhombohedral phase of $PhIO_2$, hereafter β-$PhIO_2$, was determined. Using the same approach but excluding one of the two oxygen atoms in the simulated annealing using a fragment of the α-$PhIO_2$ structure, the unknown crystal structure of PhIO could also be determined. Crystal structure data and details of the Rietveld refinement are summarized in Table 2.

The oxygen positions in both structures are associated with high uncertainty due to poor contrast with the neighboring iodine atoms. The fit for the PhIO structure was improved by restraining the intramolecular I–O distance (2.04 Å), the intermolecular I···O distance (2.37 Å) and the I–O–I bond angle (114°) determined by K-edge EXAFS (Fig. 5a and b).[5] The closest I···I distances are respectively 3.72 Å, 3.72 Å, 3.93 Å, 4.01 Å, 4.01 Å and 4.39 Å (Fig. 5c). Pleasingly this gives an average of 3.96 Å – very close to the single I···I distance of 3.95 Å that was assigned from the earlier iodine K-edge EXAFS measurements.[5] The pairing of two chains in PhIO is reflected by the crystal symmetry and a 2_1-axis along the *b*-axis. The $[I–O···I–O···]_n$ chains are found in layers which are separated by a double layer of phenyl groups parallel to the *c*-axis (Fig. 5a and d). The phenyl groups are tilted relative to each other; an *ortho* C–H group points towards the middle of the adjacent phenyl ring. The distance between the centroid of the phenyl ring and the H atom of this C–H group is 2.66 Å and the angle between the planes of the two rings is approx. 142 ± 5°. The additive effect of these supramolecular interactions provides an obvious explanation for the extreme insolubility of PhIO.

Table 2 X-ray structural data and details of Rietveld refinements for PhIO and β-$PhIO_2$ as X-ray structural data for α-$PhIO_2$

	PhIO	α-$PhIO_2$ [a]	β-$PhIO_2$
Crystal structure data			
Symmetry	Monoclinic	Monoclinic	Rhombohedral
Space group	$P2_1/c$	$P2_1$	$R3c$
a (Å)	14.306(4)	12.9041(23)	23.141(2)
b (Å)	5.868(1)	6.4023(14)	23.141(2)
c (Å)	7.407(4)	4.0115(7)	6.4155(2)
α (°)	90	90	90
β (°)	101.04(3)	99.018	90
γ (°)	90	90	120
Volume (Å^3)	610.3(3)	327.32	2975.4(2)
Z	4	2	18
Rietveld refinement			
Refined profile range (°2*θ*)	3–100		5–110
Step size (°2*θ*)	0.01		0.01
Number of structural parameters	15		16
Number of profile parameters	7		7
Number of background parameters	20		25
Number of restraints	3		5
R_p (%)	7.10		6.73
R_{wp} (%)	6.43		9.71
R_{Bragg} (%)	10.35		10.81

[a] Data for α-$PhIO_2$,[8] CCDC ref. code: IODYBZ.[3]

The extracted k^3-weighted L_3-iodine EXAFS spectrum and the modulus of the phase-corrected Fourier transform of β-$PhIO_2$ are shown in Fig. 6. Restraints for I–O distances were provided by analysis of the spectrum and those for O–I–O and C–I–O angles were derived from a survey of the solid structures of 23 iodyl compounds (ESI Fig. S5 and S6†). Intra- and intermolecular I–O bonds for α-$PhIO_2$ and β-$PhIO_2$ along with pertinent angles, torsion angles and Debye–Waller factors, $2\sigma^2$ are compared in Table 3. Only intramolecular bond distances are refined due to the limited *k*-space resolution of the L_3-edge spectrum. The residual *R*-value, as defined by Binsted *et al.*[9] was 12.7.

The crystal structures of α-$PhIO_2$ [8] and β-$PhIO_2$ are compared in Fig. 7. Strong intermolecular O···I halogen bonding between the monomers resulting in the formation of a chain similar to that found in PhIO (Fig. 5a) is a feature for both phases (Fig. 7a); however the crystal packing of these chains differs dramatically. For both structures the plane through the two O atoms and I atom of the iodyl group is perpendicular to the plane of the phenyl group. The oxygen atoms are located above and below the phenyl plane, Fig. 7b. Intramolecular I–O bonds in β-$PhIO_2$ are 0.2(5) Å shorter than that for α-$PhIO_2$ and on average the intermolecular I···O halogen bonds are slightly longer for β-$PhIO_2$ compared to α-$PhIO_2$ (2.76 Å *vs.* 2.66 Å). The environments around the iodyl unit in both structures are similar with three oxygen donor atoms from adjacent iodyl units furnishing I···O halogen bonds (Fig. 7c). Furthermore, a sphere of iodine

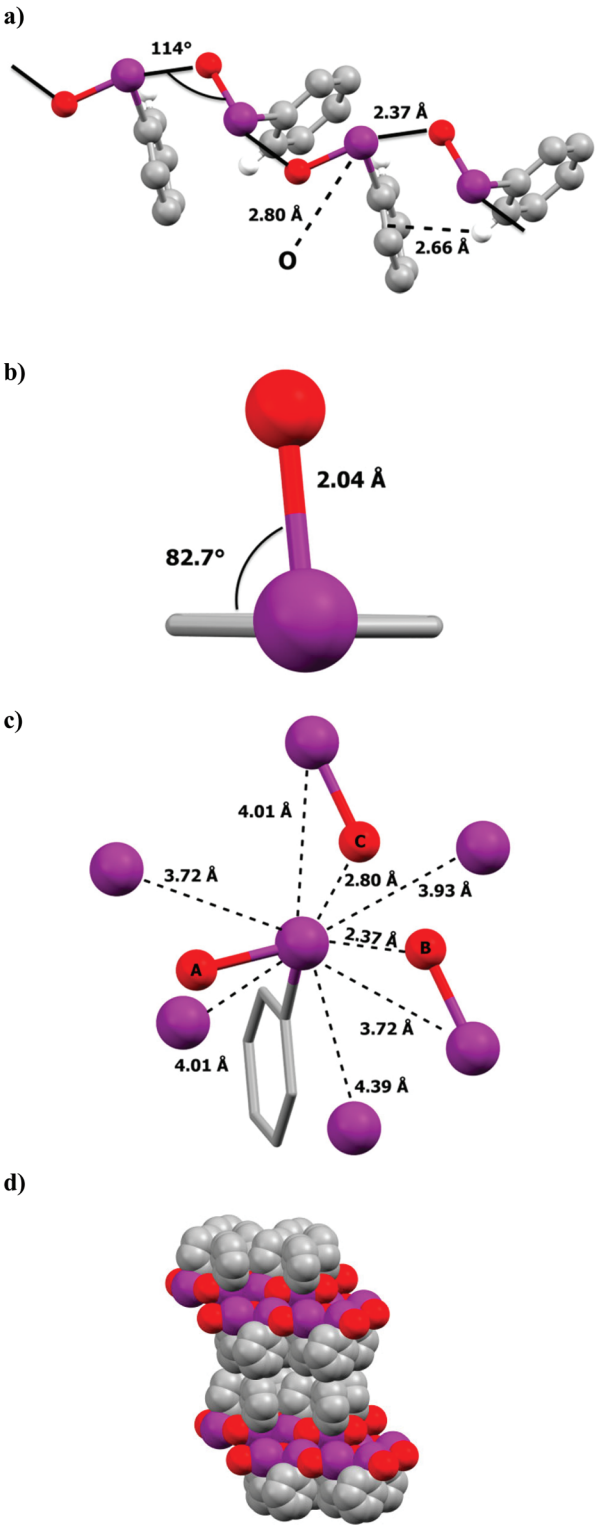

Fig. 5 Crystal structure of PhIO. (a) Halogen bonded chain along the *c*-axis. The intra-chain halogen bond (solid line), the I–O···I angle (114°) between iodosyl groups within one chain, the hydrogen atom participating in the π···H–C intra-chain interaction (dashed line) and the inter-chain O···I distance (dashed line) are shown. (b) Intramolecular I–O distance and the torsion angles I–O–C_{ipso}–C around the iodosyl group. (c) Intermolecular I···O and I···I bonds around the iodine atom of the iodosyl group. The intra O^A–I···O^B chain angle is 162.9° and the inter O^A–I···O^C chain angle is 112.9°. (d) The packing of PhIO showing layers of $[I–O···I–O···]_n$ chains.

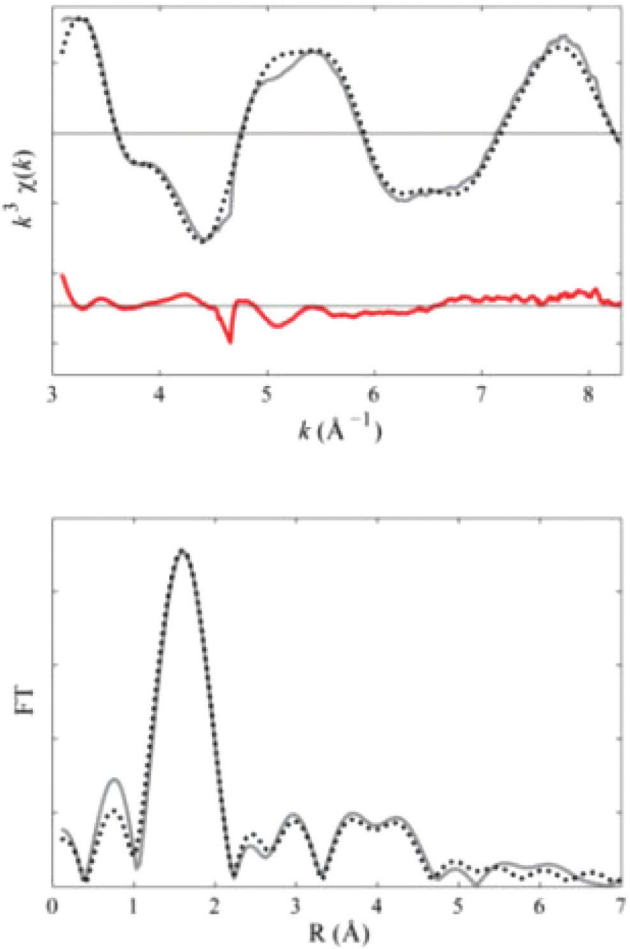

Fig. 6 k^3-Weighted L_3-iodine EXAFS spectrum (top) and the radial distribution function calculated as the modulus of the phase-corrected Fourier transform of β-$PhIO_2$ (bottom). Experimental patterns are shown in grey (full line) and calculated as dashed lines. The difference spectrum is shown in red.

Table 3 Comparison of selected X-ray structural data for α-$PhIO_2$ and β-$PhIO_2$. Distances are given in Å, angles and torsion angles are given in degrees (°)

	Crystal structure		EXAFS	
	α-$PhIO_2$	β-$PhIO_2$	R (Å)	$2\sigma^2$ (Å^2)
I–C	2.01	2.10	2.109(8)	0.002(1)
I–O	1.92	1.78[a]	1.783(4)	0.006(1)
I–O	2.02	1.78[a]	1.783(4)	0.006(1)
I···O	2.58	2.24	N/A	N/A
I···O	2.66	2.79	N/A	N/A
I···O	2.73	3.25	N/A	N/A
O–I–O	147.9	99.6[b]	N/A	N/A
O–I–C	76.4	95.6[c]	N/A	N/A
	91.1	95.8[c]		
O–I–C–C	52.3	40.9	80.9	N/A
	80.9	59.4	80.9	

[a] During refinement these values were restrained to the value of 1.78 Å determined from the EXAFS experiments. [b] This angle was restrained to 100° (based on CSD[3] analysis ESI Fig. S5). [c] These angles were restrained to 95.7° (based on CSD[3] analysis ESI Fig. S6).

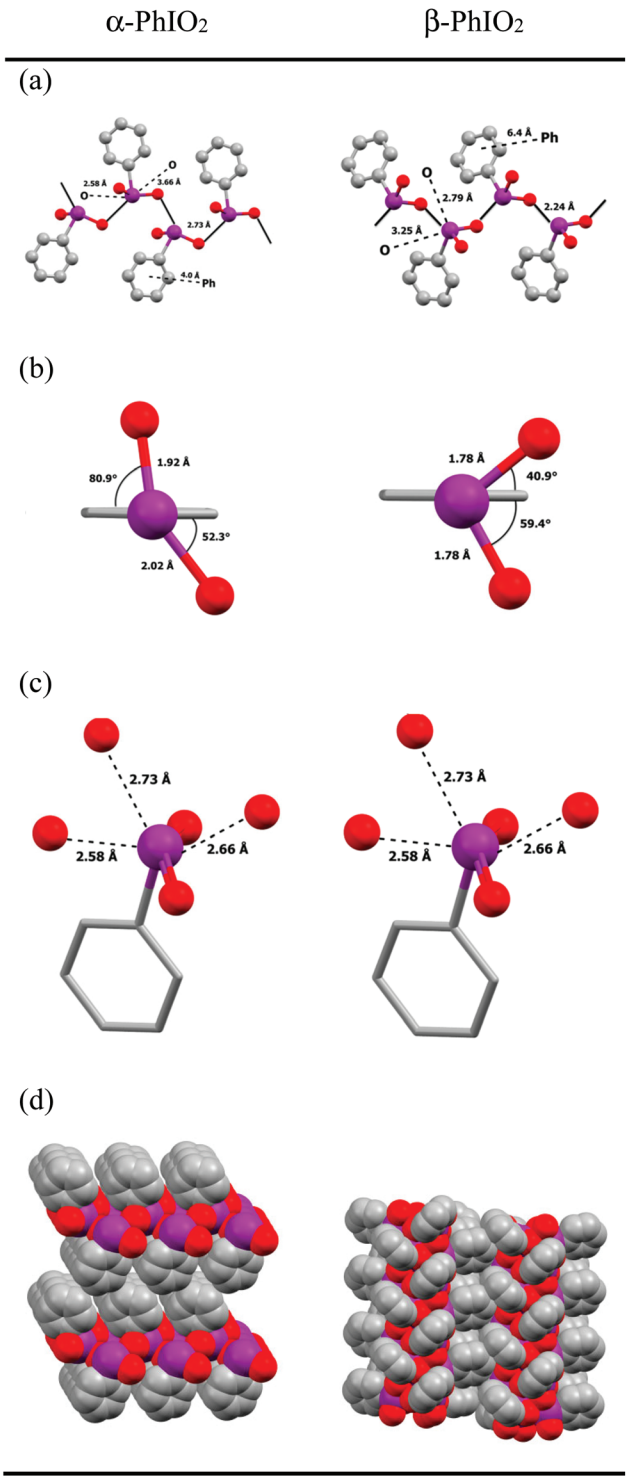

Fig. 7 Comparison of monoclinic α-$PhIO_2$ and rhombohedral β-$PhIO_2$ phases. (a) The halogen bonded chain from each structure. Intra-chain (solid black) and inter-chain (dashed black) halogen bond distances are denoted. (b) The intramolecular I–O (solid bonds) bonds and the torsion angles I–O–C–C around the iodyl group. (c) The intermolecular halogen I···O (dashed bonds) bonds around the iodyl groups. (d) The packing for the two polymorphs showing either a lamellar or a pillared structure.

atoms are located within the range of the sum of the iodine van der Waals radii (ESI Fig. S7†). α-$PhIO_2$ shows a lamellar structure with AB stacks of sheets, Fig. 7d, where $PhIO_2$ units are related through a 2-fold screw axis. The phenyl groups are stacked with the ring centroids 4.0 Å apart. The arrangement of the monomers in β-$PhIO_2$ comprises strands of three parallel $(I–O\cdots I–O)_n$ chains (Fig. 7d), whose phenyl groups point outwards forming stacks of tilted benzene rings with a distance of 6.4 Å between the centroids of the benzene units. This distance is clearly far too large to implicate any π–π bonding interactions (the distance between the layers in graphite is 3.41 Å (ref. 10)). Interactions of the π electron systems of the phenyl rings with phenyl *ortho* C–H groups from an adjacent stack are the more important supramolecular associations. The $PhIO_2$ units are related by a three-fold rotation axis. The result is pillars comprising I and O atoms parallel to the *c*-axis. β-$PhIO_2$ has a 1% larger unit cell volume per $PhIO_2$ molecule compared with α-$PhIO_2$.

It is interesting to note that (i) using the standard synthesis[11] (treatment of PhI with excess of peracetic acid) we do not prepare bulk samples of α-$PhIO_2$ and that (ii) the specific single crystal of α-$PhIO_2$ that was used for the published X-ray structure determination was not derived from such a bulk synthesis; rather it was crystal-picked from the bulk powdered product obtained from a common procedure for the synthesis of PhIO (treatment of iodobenzene dichloride with NaOH).[8] No explanation was proffered in the article about the cause of oxidation. Given the structural similarity we have found between PhIO and α-$PhIO_2$, speculation of an influence on the crystallization of α-$PhIO_2$ by a surrounding bulk of mircocrystalline PhIO seems reasonable. This might occur through a solution–solid mechanism or a solid state mechanism. Interestingly we observe bleaching of our solid samples of PhIO (stored in air-tight vials at room temperature) over months. Both XANES and PXRD reveal that these initially spectroscopically/crystalline pure samples of PhIO have converted largely to β-$PhIO_2$. However minor fractions of both PhIO and α-$PhIO_2$, as revealed by the position of the unique first Bragg peak for the patterns of PhIO, α-$PhIO_2$ and β-$PhIO_2$ are well-resolved in the pattern of the aged PhIO-sample. See overlaid powder patterns and XANES for fresh and aged PhIO, α-$PhIO_2$ and β-$PhIO_2$ in ESI Fig. S8 and S9.† Conversion of PhIO to PhI and $PhIO_2$ is known to occur by solvent mediated disproportionation in H_2O (ref. 12) and DMSO (ESI Fig. S10†). PhIO is used more commonly than $PhIO_2$ as an oxidant (counterintuitively when considering their respective iodine oxidation states). Thus, suffice it to say our observation is significant for workers utilizing PhIO as a terminal oxidant in syntheses, since the condition of the reagent may be critical. While for some oxidation reactions it is possible that both PhIO and $PhIO_2$ can be interchangeable, we observed that when attempting to oxidize substrates by $PhIO_2$ using $[Fe(tpena)]^{2+}$ as the catalyst[13] using the same conditions for which PhIO is highly effective and selective,[1] the catalytic activity decreased dramatically.

Conclusions

We have carried out iodine L_3-edge XANES on the most extensive coverage of oxidation states for iodine compounds. Satisfyingly, a linear correlation between the oxidation state and iodine L_3-edge and pre-edge energies is observed. Due to a wider spread of edge energies we show that iodine L_3-edge XANES is extremely powerful for addressing the question of the iodine oxidation state compared with the more commonly utilized K-,[14] L_1-[15,16] and L_2-[16] edges XANES and $^{127}I/^{129}I$ Mössbauer spectroscopy.[6] Of course the disadvantage is that a reliable analysis of the iodine L_3-edge EXAFS is not possible due to the interference by the overlap with the iodine L_2-edge. In this particular case, however, a single crystal X-ray structure of the unique Fe(III)-coordinated OIPh complex was available. An iodine oxidation state of +1.6 has been measured for [Fe(tpena)OIPh](ClO$_4$)$_2$ using iodine L_3-edge XANES. This suggests an inner sphere transfer of 1.4 electron equivalents to the iodine atom of the PhIO monomer, supporting the proposal that $[Fe(tpena)OIPh]^{2+}$ is a catalytically competent intermediate in homogeneous $[Fe(tpena)]^{2+}$-catalyzed sulfoxidations and epoxidation using undissolved PhIO as the terminal oxidant. Whether it is the direct oxidant or its immediate precursor cannot be ascertained by this study.

We have discovered that PhIO, a compound that has been known for one and quarter centuries[4] and described as amorphous,[5] can be microcrystalline. Building on previous EXAFS work,[5] this has allowed for its more precise structural determination using PXRD. An analysis of the structure–property relationship in the parent organic hypervalent iodine compounds PhIO and $PhIO_2$ is now possible. For the latter, our work has uncovered a new phase. In our hands this (β) phase of $PhIO_2$ is the predominant phase obtained by deliberate syntheses. For PhIO, the intra- and inter-molecular I–O bonds in polymeric PhIO, together with the C–H$\cdots\pi$ interactions between the phenyl groups in individual chains, give a clear physical explanation for the insolubility of this important reagent. While this can be impractical, this feature is inherent for the relatively long shelf life of solid state PhIO, making it advantageous for handling. That said, we can also document that aging of PhIO occurs and if this goes unnoticed it may result in poorer yields from reactions when PhIO is ostensibly used as a terminal oxidant. An important point of this work is that the development of homogeneous metal-based catalysts like $[Fe(tpena)]^{2+}$, which are able to break up polymeric PhIO to extract the potent monomeric PhIO, and even activate it further by coordination, opens up new methodologies for the catalysis of selective homogeneous oxidations.

Experimental

Iodosylbenzene (PhIO) was synthesized using a slight modification of the procedure reported by Dauban.[17] Elemental analysis calcd (%) for C_6H_5IO C: 32.76, H: 2.29, I: 57.768. Found C: 32.60, 32.69, H: 2.26, 2.24, I: 57.53, 57.74 (Atlantic Microlab Inc. Norcross GA, USA). Phenyliodine diacetate (PIDA) (2.02 g, 6.26 mmol) was placed in a 50 ml round bottomed flask and suspended in 6.7 mL of water. 8.3 mL of 4 M NaOH solution was added over a period of 5 min under vigorous agitation. The yellow heterogeneous mixture was then vigorously stirred for 30 min at room temperature, and then left without agitation for an additional 30 min. The yellow solid was isolated using a Büchner funnel and re-suspended in H_2O (40 mL). The suspension was stirred for 5 min. The product was collected on a Büchner funnel, washed with H_2O (4 × 20 mL) and dichloromethane (2 × 15 mL), and dried under vacuum overnight to afford 54% yield.

Iodylbenzene ($PhIO_2$) was synthesized by the method reported by Sharefkin[11] in 45% yield. Elemental analysis calcd (%) for $C_6H_5IO_2$ C: 30.54, H: 2.14, I: 53.77. Found C: 30.45 and 30.57, H: 2.12 and 2.12, I: 53.81 and 53.67 (Atlantic Microlab Inc. Norcross GA, USA).

Caution: potentially explosive compounds.[4]

[Fe(tpena)OIPh](ClO$_4$)$_2$ was prepared as described previously.[2] The solid is unavoidably contaminated by $[Fe_2(tpena)_2O](ClO_4)_4$ and [Fe(tpena)](ClO$_4$)$_2$.[1] Neither of these compounds contain iodide and hence do not interfere with the XANES measurements.

XAFS

XAFS experiments were performed on the MAX-II storage ring, beamline I811, MAXIV Laboratory, Lund, Sweden[18] using a Si(111) double crystal monochromator detuned 50% at 4840 eV. The neat samples were ground prior to the measurement and the sample with a suitable optical thickness was prepared and mounted in between a layer of Kapton tape. All measurements were performed at room temperature, and ion chambers before and after the samples were used to measure the incident and transmitted intensities (I_0 and I_1). Fluorescence data I_f were collected using a PIPS PD-5000 (passivated implanted planar silicon) detector from Canberra. The iron K-edge measurements were carried out in the energy range 6962 eV to 8112 eV with a scan time of 5 min per spectrum and calibrated with iron (Fe(0), E = 7112 eV). The iodine L_3-edge measurements were carried out in the energy range 4460 to 4837 eV with a scan time of 3 min per spectrum. The edge was calibrated with KI (E = 4560.8 eV). 5 to 10 successive spectra were collected on each sample and averaged. The data processing was performed using WinXAS.[19] Using the structure of α-$PhIO_2$ as an initial model,[8] modelling was carried out by EXCURVE[9,20] in which the phenyl group was kept constrained during the refinement. The intramolecular I–O distances were kept equal. Debye–Waller factors for distances involving similar atoms were grouped.

X-ray powder diffraction

Powder diffraction data were collected at room temperature for PhIO and $PhIO_2$ for respectively 16 and 13 h on a Stoe Stadi P diffractometer using Cu Kα_1 radiation (λ = 1.5406 Å). The structures were solved from the powder diffraction data using EXPO2014.[21] Indexing was performed by the NTREOR algor-

ithm implemented in EXPO.[22] Structure solution was performed by simulated annealing methods using a structure of α-$PhIO_2$ [8] as a fragment (for the structure solution of PhIO one of the two O-atoms was excluded from the searching fragment). The structures were refined by the Rietveld method using GSAS-II.[23] In addition to refinement of an overall scale factor and the 2θ-displacement, the profiles were refined by three peak broadening parameters (u, v, and w), one peak shape and one asymmetry parameter. The structural parameters refined count cell parameters, coordinates and atomic displacement factors. Due to the limited angular resolution of the diffraction peaks, the iodobenzene fragments in both PhIO as well as in β-$PhIO_2$ were refined as rigid bodies in order to minimize the number of structural parameters. By doing this the coordinates for the PhI moiety can be refined using only 5 parameters. The PhI fragment used was taken from the crystal structure of diphenyliodonium iodide.[24] Based on an analysis of relevant PhI-containing structures deposited in CSD,[3] solved at room temperature and with $R < 5\%$, this structure showed to be a good representative for the iodobenzene fragment. H-atoms were included as riding atoms. The atomic displacement factors of similar elements were set equally, and were not refined for H-atoms. Additionally due to the limited angular resolution and heavy Fourier rippling around iodine atoms the oxygen positions could not be refined without the introduction of restraints. For the PhIO structure, the I–O distances were restrained to 2.04 Å, I···O to 2.37 Å and I–O–I to 114°, according to the distance determined from the K-edge EXAFS study of PhIO by Carmalt *et al.*[5] For the β-$PhIO_2$ structure, the intramolecular I–O distances were restrained to 1.78 Å, which is the distance determined by EXAFS. The intermolecular O–I–O and C–I–O angles were restrained to 100.0° and 95.7°, respectively, based on a CSD-survey (see ESI Fig. S5 and S6†).

Acknowledgements

Dr Stefan Carlsson, a beamline scientist at MAX Lab Synchrotron source, Lund, Sweden. Support from the Danish Council for Independent Research|Natural Sciences (grant 4181-00329 to CMcK) and DANSCATT. Ms Vibe Jakobsen and Mr David Poulsen de Sousa for help with XANES measurements. Dr Daniel Strand, Kemicentrum, the University of Lund, Sweden, for samples of PIDA, DMP and H_5IO_6.

References

1 D. P. de Sousa, C. Wegeberg, M. S. Vad, S. Mørup, C. Frandsen, W. A. Donald and C. J. McKenzie, *Chem. – Eur. J.*, 2016, **22**, 3810–3820.
2 A. Lennartson and C. J. McKenzie, *Angew. Chem., Int. Ed.*, 2012, **51**, 6767–6770.
3 F. H. Allen, *Acta Crystallogr., Sect. B: Struct. Sci.*, 2002, **58**, 380–388.
4 C. Willgerodt, *Ber.*, 1892, **25**, 3494–3502.
5 C. J. Carmalt, J. G. Crossley, J. G. Knight, P. Lightfoot, A. Martin, M. P. Muldowney, N. C. Norman and A. G. Orpen, *J. Chem. Soc., Chem. Commun.*, 1994, **20**, 2367–2368.
6 B. S. Ehrlich and M. Kaplan, *J. Chem. Phys.*, 1971, **54**, 612–620.
7 Solid samples of $[Fe(tpena)(OIPh)](ClO_4)_2$ are reactive and hence difficult to isolate. Hence they are unavoidably contaminated by the iron(III) complexes $[(tpenaH)Fe(\mu\text{-}O)Fe(tpenaH)](ClO_4)_4$ and $[Fe(tpena)](ClO_4)_2$ from which they are prepared. Neither of these parent compounds however contain iodide. The sample used for the Fe K-edge XANES measurement contains the maximum concentration we could achieve (*ca.* 60%) of $[Fe(tpena)(OIPh)](ClO_4)_2$. At this concentration if the Fe oxidation state for this was higher than +3 this would be manifested by absorption at a higher energy. For reference we measured the edges of pure samples of $[(tpenaH)Fe(\mu\text{-}O)Fe(tpenaH)](ClO_4)_4$ and $[Fe(tpena)](ClO_4)_2$ and a solution state sample of the iron(IV) compound $[(FeO(tpenaH)]^{2+}$. See ESI Fig. S4.†
8 N. W. Alcock and J. F. Sawyer, *J. Chem. Soc., Dalton Trans.*, 1980, 115–120. CCDC ref. code: IODYBZ.
9 N. Binsted, R. W. Strange and S. S. Hasnain, *Biochemistry*, 1992, **31**, 12117–12125.
10 O. Hassel and H. Mark, *Z. Phys.*, 1924, **25**, 317.
11 J. G. Sharefkin and H. Saltzman, *Org. Synth. Coll.*, 1963, **43**, 65.
12 C. Willgerodt, *Ber.*, 1893, **26**, 1307–1313.
13 Oxidative catalysis of thioanisole by 10 mol% $[Fe(tpena)]^{2+}$ in MeCN at rt using either PhIO or $PhIO_2$ as the stoichiometric terminal oxidant, shows that after 2 h using PhIO as the oxidant, thioanisole is fully converted to methyl phenyl sulfoxide, whereas 20% of the thioanisole is still not converted even after 18 h using $PhIO_2$. Methyl phenyl sulfone is not observed with either of the oxidants. ^{1}H NMR was used for quantification.
14 (*a*) Y. S. Shimamoto and Y. Takahashi, *Anal. Sci.*, 2008, **24**, 405–409; (*b*) D. Laurencin, D. Vantelon, V. Briois, C. Gervais, A. Coulon, A. Grandjean and L. Campayo, *RSC Adv.*, 2014, **4**, 14700–14707; (*c*) D. A. McKeown, I. S. Muller and I. L. Pegg, *J. Nucl. Mater.*, 2015, **456**, 182–191; (*d*) B. J. Riley, M. J. Schweiger, D.-S. Kim, W. W. Lukens Jr., B. D. Williams, C. Iovin, C. P. Rodriguez, N. R. Overman, M. E. Bowden, D. R. Dixon, J. V. Crum, J. S. McCloy and A. A. Kruger, *J. Nucl. Mater.*, 2014, **452**, 178–188; (*e*) Y. S. Shimamoto, Y. Takahashi and Y. Terada, *Environ. Sci. Technol.*, 2011, **45**, 2086–2092; (*f*) N. Yamaguchi, M. Nakano, R. Takamatsu and H. Tanida, *J. Environ. Radioact.*, 2010, **101**, 451–457; (*g*) M. C. Feiters, F. C. Küpper and W. Meyer-Klaucke, *J. Synchrotron Radiat.*, 2005, **12**, 85–93; (*h*) W. A. Reed, I. May, F. R. Livens, J. M. Charnock, A. P. Jeapes, M. Gresley, R. M. Mitchell and P. Knight, *J. Anal. At. Spectrom.*, 2002, **17**, 541–543.
15 Y. Jung, S.-J. Hwang and S.-J. Kim, *J. Phys. Chem. C*, 2007, **111**, 10181–10184.

16 T. Konishi, W. Tanaka, T. Kawai and T. Fujikawa, *J. Synchrotron Radiat.*, 2001, **8**, 737–739.
17 P. Dauban, L. Sanière, A. Tarrade and R. H. Dodd, *J. Am. Chem. Soc.*, 2001, **123**, 7707–7708.
18 S. Carlson, M. Clausén, L. Gridneva, B. Sommarin and C. Svensson, *J. Synchrotron. Radiat.*, 2006, **13**, 359–364.
19 T. Ressler, *J. Synchrotron Radiat.*, 1998, **5**, 118–122.
20 (*a*) S. J. Gurman, N. Binsted and I. Ross, *J. Phys.*, 1984, **C17**, 143–151; (*b*) S. J. Gurman, N. Binsted and I. Ross, *J. Phys.*, 1986, **C19**, 1845–1861.
21 (*a*) A. Altomare, M. Camalli, C. Cuocci, C. Giacovazzo, A. Moliterni and R. Rizzi, *J. Appl. Crystallogr.*, 2009, **42**, 1197–1202; (*b*) A. Altomare, C. Cuocci, C. Giacovazzo, A. Moliterni, R. Rizzi, N. Corriero and A. Falcicchio, *J. Appl. Crystallogr.*, 2013, **46**, 1231–1235.
22 A. Altomare, C. Giacovazzo, A. Guagliardi, A. G. G. Moliterni, R. Rizzi and P.-E. Werner, *J. Appl. Crystallogr.*, 2000, **33**, 1180–1186.
23 B. H. Toby and R. B. Von Dreele, *J. Appl. Crystallogr.*, 2013, **46**, 544–549.
24 N. W. Alcock and R. M. Countryman, *J. Chem. Soc., Dalton Trans.*, 1977, **3**, 217–219.